Dynamic Fracture Properties of Modified S-FPZ Model for Concrete

Jung-Heum Yon[1] and Min-Kuk Seo[2]

Abstract: The fracture energy evaluated from the previous experimental results can be simulated by using the modified singular fracture process zone (S-FPZ) model. The fracture model has two fracture properties of strain energy release rate for crack extension and crack close stress versus crack width relationship $f_{ccs}(w)$ for fracture process zone (FPZ) development. The $f_{ccs}(w)$ relationship is not sensitive to specimen geometry and crack velocity. The fracture energy rate in the FPZ increases linearly with crack extension until the FPZ is fully developed. The fracture criterion of the strain energy release rate depends on specimen geometry and crack velocity as a function of crack extension. The behaviors of micro-cracking, micro-crack localization and full development of the FPZ in concrete can be explained theoretically with the variation of strain energy release rate with crack extension.

Keywords: concrete, crack velocity, fracture criterion, fracture energy, fracture process zone, specimen geometry

1. Introduction

Current research of the concrete dynamic fracture are limited to measuring a constant fracture criterion for crack extension such as stress intensity factor of the linear elastic fracture mechanics (LEFM), the maximum crack closure stress (CCS) of the fictitious crack model[1] and the crack band model[2]. However, the experimental results observed by using acoustic emission[3-5] and electron microscopy[6] have shown the existence of micro-cracking and micro-crack localizing processes. The initial distribution of the micro-cracks and the localization of the propagating micro-cracks may need different fracture criteria for crack extension of an assumed discrete crack.[7]

The singular fracture process zone (S-FPZ) model[8] was proposed to explain the parabolic crack tip opening observed by the laser holographic interferometry[9] and dynamic Moire interferometry[10] tests. The crack opening shape implied a crack-tip singularity for a rapidly propagating crack. The S-FPZ model assumes a constant strain energy release rate or stress intensity factor as a fracture criterion, and then that tip is trailed by the fracture process zone (FPZ). To simulate the macro-cracking and the micro-crack localization, the S-FPZ model is modified in this study. In the modified S-FPZ model, the fracture criterion of strain energy release rate is assumed as a function of crack extension.

In this study, the energy dissipation mechanism governing the measured dynamic responses of small size three-point bend (TPB) specimens and large size crack-line wedge-loaded double-

[1] KCI member, Dept. of Civil Engineering, Inha University, Inchon 402-751, Korea. *E-mail: jyon@inha.ac.kr*

[2] KCI member, Dept. of Civil Engineering, Inha University, Inchon 402-751, Korea.

cantilever beam (CLWL-DCB) specimens has been investigated by applying the energy balance to the modified S-FPZ model. The fracture properties of the modified S-FPZ model such as the strain energy release rate and the CCS versus crack opening displacement (COD) relation in the FPZ is determined from the required fracture energy of the experimental results.[11,12] The effects of the specimen geometries and crack velocities have been analyzed with the optimized fracture properties and the energy dissipation mechanism. The concrete cracks take time to develop fully, and it is to be expected that cracks propagate at a relatively low velocity for dynamic loading.[13] Therefore, the effect of stress wave in concrete has not been considered in this study.

2. Fracture analysis of concrete

The fracture behavior of concrete shows the process of micro-crack extension, micro-crack localizing due to bridging, and macro-crack extension. To analyze this complicated behavior, the finite element method (FEM) should be used, and simple equation of the fracture properties should be derived. The study of the concrete fracture behavior needs the understanding of cracking procedures and the development of models for numerical analysis.

For numerical analysis of concrete fracture behavior, the smeared crack band model (CBM)[2] are used widely to plain and reinforced concrete. In this model, the tensile stiffness of a smeared element as a continuum is decreased by increasing deformation. A discrete crack of the fictitious crack model (FCM)[1] is simulated by releasing constrained nodes along the expected crack paths, and a spring element connecting the released nodes is used for the tensile stiffness of the FPZ as shown in Fig. 1.

The fracture criterion of both fracture models is the tensile

● Constrained node   -\/\/\/\/- Spring element
○ Released node
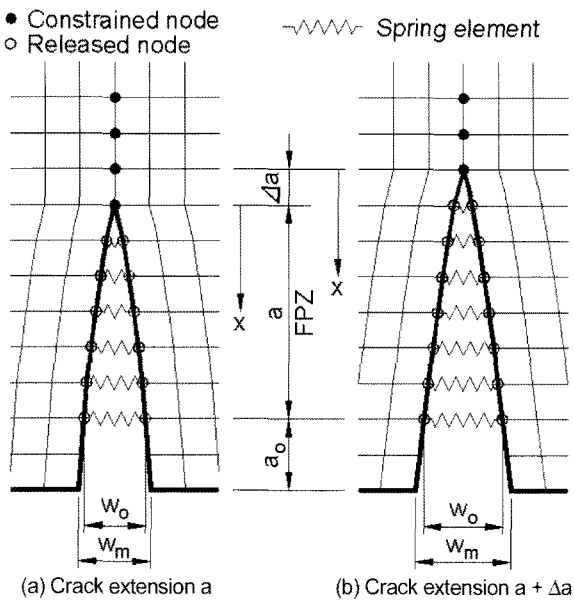
(a) Crack extension a

(b) Crack extension a + Δa

Fig. 1 FEM modeling of a discrete crack.

strength defined as the maximum crack closure stress or tensile strength. However, the stress of a crack tip element is depended upon the size of a finite element, since the boundary condition changes suddenly at the crack tip. Therefore, the stress of a finite crack tip element is under-estimated, and deformation can be stiffened by continuing the stress distribution. In this section, the numerical analysis of a discrete crack under the concept of energy balancing[14,15] is introduced, and the fracture properties of concrete are analyzed by the energy balancing.

2.1 Fracture criterions of fracture models

For crack propagation, enough amounts of strain energy should be stored locally. When stored energy reaches a critical value, a crack starts on propagation. The critical energy can be estimated from the difference of strain energy at the intial crack size α and an extension $\Delta\alpha$ as shown in Fig. 1 with a constant load or load-point displacement. The variation of the strain energy E_s is defined as the fracture energy E_f for crack extension $\Delta\alpha$ and it can be estimated as following:

$$E_f(\alpha) = E_s(\alpha) - E_s(\alpha + \Delta\alpha) \tag{1}$$

By using the fracture energy rate G_f defined as energy required to propagate a crack of unit area, eq. (1) can be expressed more generally such as,

$$G_f(\alpha) = G(\alpha) + G_{fpz}(\alpha) = \frac{E_f(\alpha)}{t\Delta a} \tag{2}$$

where, G is the strain energy release rate for crack extension of unit area, G_{fpz} is the fracture energy rate required to develop the FPZ, and t is the thickness of the crack.

Eq. (2) can be applied to the LEFM of a brittle material with $G_{fpz} = 0$, and to the CBM and the FCM with $G = 0$. When the strain energy release rate G in eq. (2) reaches the critical value G_c, the crack starts on propagating. In the LEFM, the G_c is a fracture property independent of the crack size and stress condition. By using the energy concept of eq. (2), the fracture

criterion of a crack tip element can be easily determined rather than using singular elements or quarter-point element,[16] which need relatively large node numbers and a complicate strain-displacement matrix.

For a composite material such as concrete, the concept of the FPZ should be applied to simulate the micro-crack propagation, micro-crack localizing and bridging, and macro-crack propagation. Since the FCM and CBM assume continuous distribution of the stress front and rear a crack tip, the fracture criterion should be the maximum CCS of the FPZ. The S-FPZ model allows discontinuous stress distribution at a crack tip, and then applies the G_c as a fracture criterion. And the modified S-FPZ model assumed that the fracture criterion G_c is a function of the crack extension.

2.2 Fracture energy rate in FPZ

The fracture energy is usually defined as the energy required for the fully development of the unit area FPZ. However, in this study, the term of the fracture energy density is used for the energy to distinguish from the energy required for the total crack surface of a specimen. The fracture energy density is integral of the CCS-COD relation $f_{ccs}(w)$ in Fig. 2 as following:[7]

$$G_{FPZ} = \int_0^{w_c} f_{ccs}(w)dw \tag{3}$$

where w_c is the critical COD defined as the maximum COD which can transfer tensile stress.

After crack propagation, the fracture energy rate $G_{fpz}(w_x)$ required for the development of the FPZ until the crack tip opening width w_x may be calculated from the dark area in Fig. 2 such as,

$$G_{fpz}(w_x) = \int_0^{w_x} f_{ccs}(w)dw - \frac{1}{2}f_{ccs}(w_x)w_x \tag{4}$$

In eq. (4), the permanent deformation is not considered since the wedge action can be expected due to the particle movements on the crack surfaces during unloading, it can generate the additional strain energy of a different energy dissipation mechanism.[7] The energy required to develop the FPZ is computed as following equation:

$$E_{fpz}(a) = \int_0^a G_{fpz}(w_x)t dx = \sum_j G_{fpz}(w_j)t_j\Delta a_j \tag{5}$$

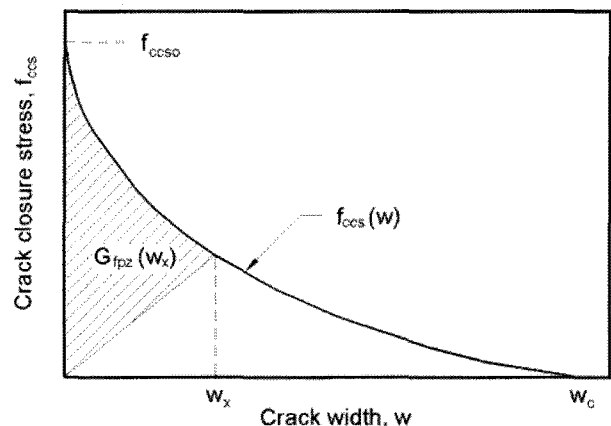**Fig. 2** f_{ccs} (w) and fracture energy rate in FPZ.

where the notation j indicates the released node number, and w_j, t_j and Δa_j are the COD, thickness and element size of the node j. For the calculation of eq. (5), the COD w_x should be expressed as a function of the distance x from the crack tip such as Fig. 1. The fracture energy G_{fpz} rate in eq. (4) can be defined from the fracture energies E_{fpz} of the spring elements between the crack sizes of a and $a + \Delta a$ as following:

$$G_{\text{fpz}}(a) = \frac{E_{\text{fpz}}(a + \Delta a) - E_{\text{fpz}}(a)}{t\Delta a} \tag{6}$$

2.3 Fracture properties of discrete crack

The critical strain energy release rate G_c as the fracture criterion of brittle material is the strain energy released for creation of the unit area crack surface at a singular crack tip. The G_c of the brittle material is the only fracture property independent of crack length, loading and geometry conditions. If the stress distribution front and rear the crack tip is continuous, the CCS-COD relation should be given as the fracture property and the maximum CCS f_{ccso} in Fig. 2 can be used as a fracture criterion, since the singularity can not occur such as $G_c = 0$. However, in the FEM, the simulation of the continuous stress distribution at a crack tip generated by releasing nodes is very difficult.

When the FPZ exists behind a crack tip, the extension of the FPZ needs more energy for crack propagation. The increasing CCS, which restrains the crack width, can increase the G_c. Therefore, the following fracture properties should be given to analyze the fracture behavior with the FEM.

① Strain energy release rate $G(a)$
② CCS-COD relation in the FPZ $f_{\text{ccs}}(w)$

The external work at each crack extension a is calculated from the measured external loads and loading-point displacements, and the kinematic energy is estimated by the integral of the inertial force versus displacement relation. The strain energy can be calculated from the external load excluding the inertial force. The fracture energy at the crack extension a is the difference between the external work excluding the kinematic energy and the strain energy.[12]

To estimate the fracture properties of concrete from the experimentally determined crack extension and fracture energy, the distribution of crack opening should be defined by using eqs. (4)–(6). In the static crack propagation of the modified S-FPZ model, the distribution of crack opening at crack extension a was assumed as the following equation:

$$w(x) = w_x = w_0\left(\frac{x}{a}\right)^\beta \tag{7}$$

where w_0 is the crack tip opening width (CTW), which can be estimated from the measured crack mouth width (CMW), and β is the crack opening shape factor.

### 3. Experimental results of dynamic fracture behaviors

In this study, the fracture properties of the modified S-FPZ model were estimated from the experimental results of the dynamic TPB tests[11] and CLWL-DCB tests.[12] The specimen geometries and loading conditions are shown in Fig. 3. The responses of the TPB and CLWL-DCB tests were measured until

the crack extension of 102 mm and 381 mm, respectively.

Fig. 4 shows the histories of the load and load-point displacement, and Fig. 5 shows the crack extension histories measured by using the strain gages in Fig. 3. The crack velocities at the failure were 0.00016~65.8 mm/s for the TPB test and 0.0008~215 m/s for the CLWL-DCB tests. The loads of both tests and the CMW of the TPB tests in Fig. 3 are shown in Fig. 6 for the load-point relation. The load versus load-point displacement relations were used to calculate the external work, kinetic energy and strain energy, and the CMW versus load-point displacement
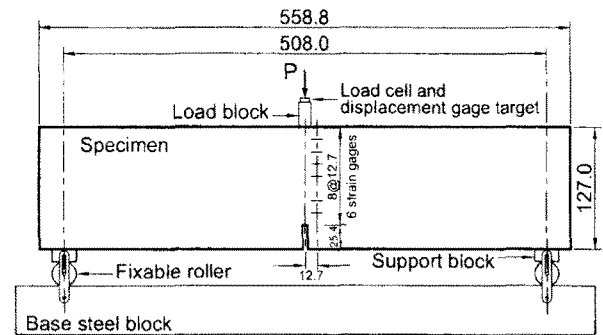
(a) TPB specimen [11]
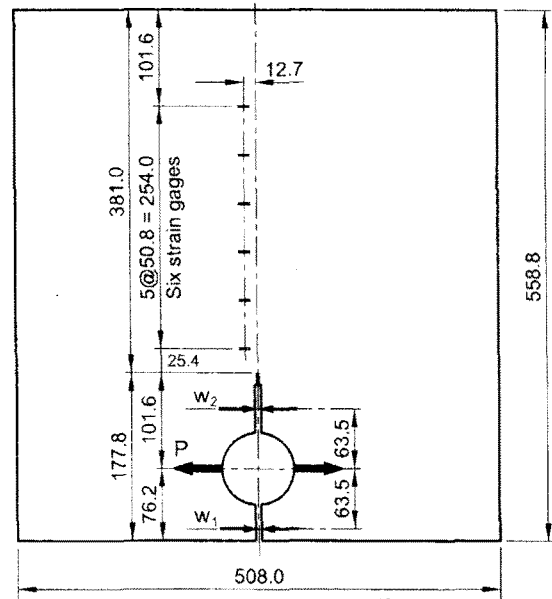
(b) CLWL-DCB specimen [12]

Thickness = 50.8 mm   Unit: mm

Fig. 3 Configurations of test specimens[7].
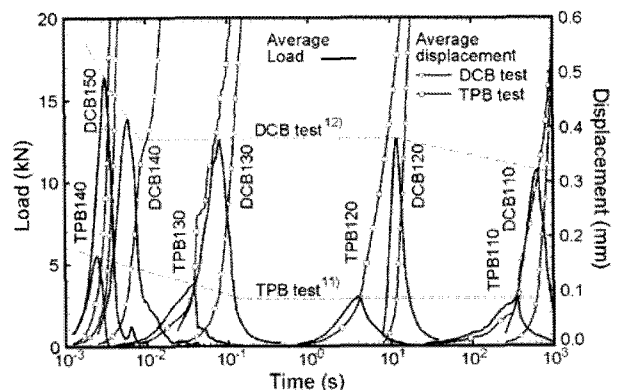

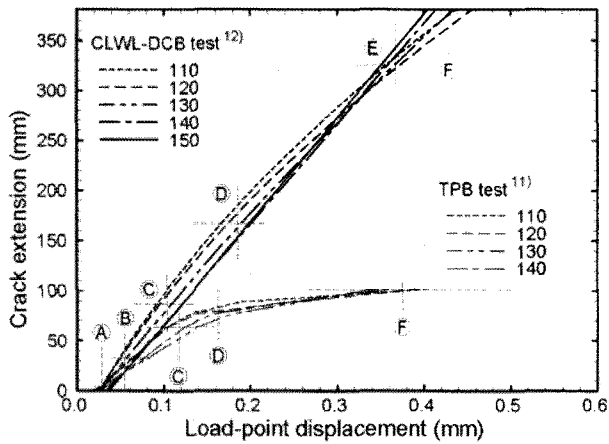**Fig. 4** Average measured and load-point displacement histories.
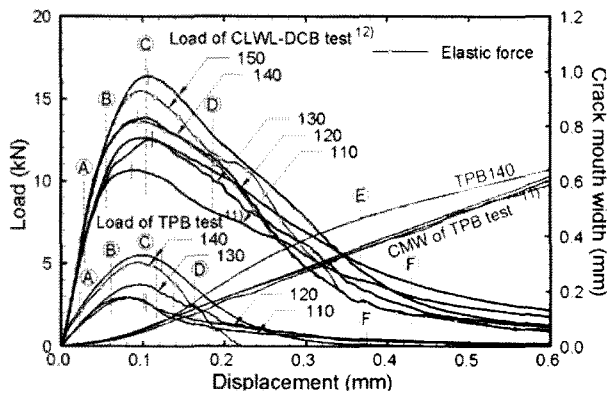
Fig. 5 Average measured crack extensions.

Fig. 6 Average measured load and crack mouth width.

relations for the crack opening shape factor.

The summaries of both specimen tests are listed in Table 1. In Table 1, the period is the time when specimen failed perfectly. The fracture energy rate G_F was estimated by dividing the average external work not including kinematic energy by the crack surface area. The variation of the G_F was not very sensitive

Table 1 Average experimental results of TPB and CLWL-DCB tests.[11,12]

Test No.		Period (s)	Peak load (kN)	Work (N · m)	G_F (N/m)
TPB	TPB110	1,952	2.961	0.579	112
	TPB120	20.06	2.994	0.607	117
	TPB130	0.164	3.786	0.691	134
			3.683*	0.691*	134*
	TPB140	0.00345	5.462	0.797	154
			5.053*	0.646*	125*
CLWL-DCB	DCB110	1,302	10.66	4.027	208
	DCB120	35.74	12.66	5.370	277
	DCB130	0.441	12.51	4.138	214
	DCB140	0.0432	13.97	4.112	212
			13.53*	4.058*	210*
	DCB150	0.00518	16.28	4.631	239
			15.49*	4.424*	229*

* Responses excluding inertial force.

to the crack velocity, but it was sensitive to the specimen geometry.

Figs. 7 and 8 shows the fracture energies required for the measured data, and they were estimated by eqs. (1) and (2) in References 11 and 12. In Fig. 7, the fracture energies of the CLWL-DCB specimens are also shown to compare the fracture energies of both specimens at relatively small crack extensions. Initially, the facture energies of the CLWL-DCB tests were larger than those of the TPB tests, but the fracture energy of the TPB140 test increased suddenly after Step ©.

4. Dynamic fracture properties of modified S-FPZ model

In this study, the fracture properties of $G(a)$ and $f_{ccs}(w)$,which should satisfy the fracture energies in Figs. 7 and 8, were estimated to minimize the standard error to the fracture energy rates computed by eq. (2).[7] The computation of the fracture energies based on the following procedure of Reference 7 for the static crack propagation. In the static crack propagation, the initial crack tip width w_0 and crack opening shape factor β were assumed as the following equations:

$$\frac{w_o}{w_m} = \frac{1}{1 + \beta(a_o/a)} \tag{8}$$

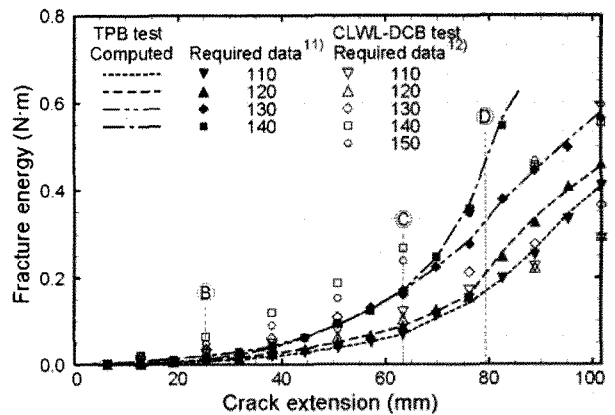$$\beta = \frac{a\Delta w}{\Delta a_w w_m - a_o \Delta w} \tag{9}$$

Fig. 7 Required and computed fracture energies of TPB tests.
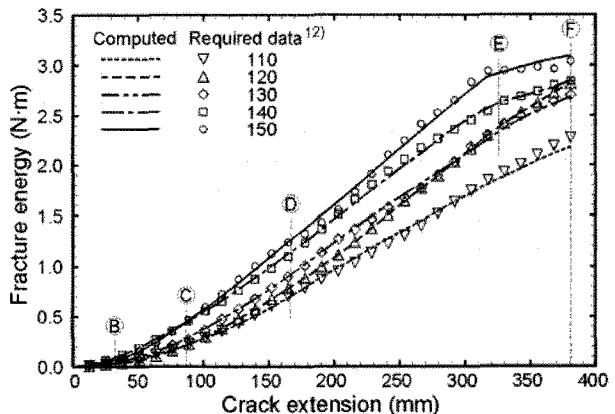

Fig. 8 Required and computed fracture energies of CLWL-DCB tests.

where w_m is the crack mouth width at the crack extension a, a_o is the initial crack size, Δw is the difference of crack widths at w_1 and w_2 separated by the distance Δa_w in Fig. 3.

A crack opening width can be calculated by using eq. (7) with the parameters of eqs. (8) and (9). The fracture energy at crack extension a is calculated by the following integration:

$$E_f(a) = \int_0^a [G(x) + G_{fpz}(w_x)] t\, dx \tag{10}$$

The curve in Figs. 7 and 8 was the fracture energy of each test computed by using eq. (10) with the parameters in Figs. 9~11 and Table 2.

The critical strain energy release rates in Fig. 10 and the CCS-COD relations summarized in Fig. 11 and Table 2 were determined to minimize the standard error of the computed fracture energies by using eq. (10) to the estimated fracture energies for the measured data at each crack extension. During
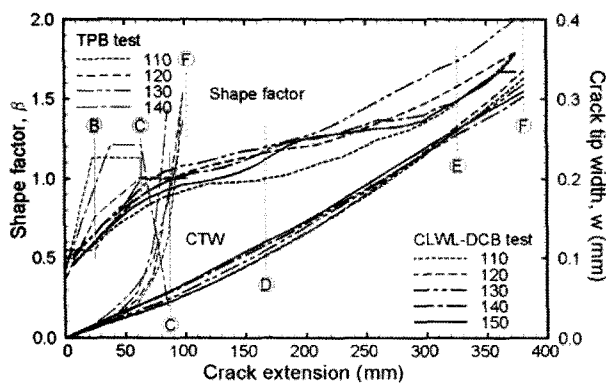

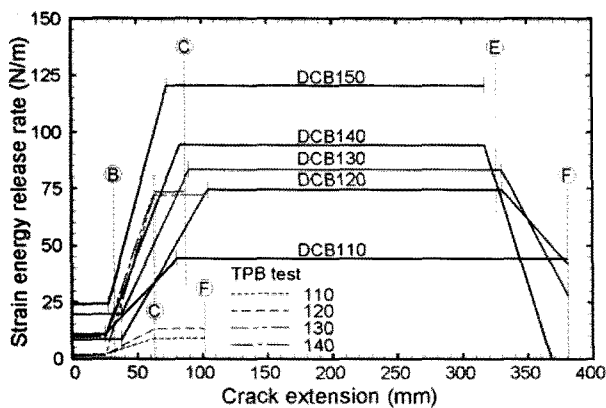Fig. 9 Estimated shape factors and crack tip widths.
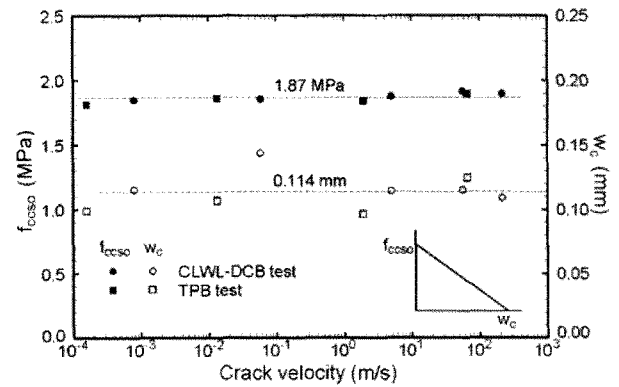

Fig. 10 Applied strain energy release rates.

Fig. 11 Applied crack closure stresses and crack width relationships

the optimizing procedure, the crack opening shape factors and the initial crack tip opening widths of the TPB tests were also determined. The crack opening shape factors of the CLWL-DCB tests were estimated by using eq. (9) for the measured crack opening widths of w_1 and w_2. The standard error of this study were less than 3 percents as shown in Table 2.

The shape factors of the TPB tests at the initial crack extension are about 0.5 as shown in Fig. 9, and then the shape factors of TPB110 and TPB140 tests increases to about 1.2, whereas the shape factors of TPB120 and TPB130 tests similar to the CLWL-DCB tests increases to 1.0. The shape factors of all TPB tests after Step © are 1.0 except the TPB140 tests in which rigid motion may be expected. The increasing rate of the crack tip width for the TPB tests at Step © is much larger than that of the CLWL-DCB tests. The initial shape factor 0.5 of the CLWL-DCB tests increased to 1.0 at Step © by crack extension, and it remains roughly constant until Step ⑩. The shape factor less than 1.0 indicates a blunt crack opening shape, so that singularity should be required at a discrete crack tip as the results of the laser holographic interferometry[9] and the moire interferometry[10] tests.

Fig. 10 shows the applied G as the fracture criterion in this study. The constant value of G_{min} increases at Step ⑧, and G reaches the maximum value of G_{max} in Table 2 at Step ©. In the dynamic CLWL-DCB tests, the value of G decreases at Step ⑤. Therefore, Steps ⑧, © and ⑤ of each group are determined from G for the crack extension. The average crack extensions of the TPB and CLWL-DCB tests at Step ⑧ are 25.4 mm and 32.4 mm, respectively, and those at Step © are 63.5 mm and 87.2 mm, respectively. The crack extensions and load-point displacements of the steps are summarized in Table 3.

The constant G before Step ⑧ may indicate the unconnected

Table 2 Average measured crack velocities and applied fracture properties.

Property	TPB test				CLWL-DCB test				
	110	120	130	140	110	120	130	140	150
a_{ave} (m/s)[1]	0.00016	0.0134	1.92	65.8	0.0008	0.0589	4.95	56.3	215
f_{ccso} (MPa)	1.81	1.86	1.84	1.90	1.85	1.85	1.88	1.92	1.90
w_c (mm)	0.0991	0.1067	0.0965	0.1245	0.115	0.143	0.114	0.115	0.109
G_{FPZ} (N/m)	89.8	99.3	88.8	118.0	106.5	133.3	107.2	110.0	103.1
G_{min} (N/m)	1.93	1.82	1.58	9.81	10.65	8.48	19.65	9.56	24.10
G_{max} (N/m)	9.11	13.31	72.33	73.73	44.24	74.60	83.36	94.22	120.49
Standard error (%)[2]	3.00	2.17	2.52	1.02	2.93	2.18	2.01	1.98	2.59

[1] Average crack velocity during crack extension
[2] Standard error of the computed fracture energies to the required fracture energies for tests

and widely distributed micro-cracking, and the increasing G between Steps Ⓑ and Ⓒ could be the result of the micro-crack localizing observed in Reference 6. Step Ⓒ of the TPB tests occurs at the maximum strain energy,[11] but Step Ⓒ of the CLWL-DCB tests occurs at the peak load in Fig. 6. The increasing rate of the dynamic G of the TPB tests between Steps Ⓑ and Ⓒ is similar to that of the CLWL-DCB tests, but G_{max} of the TPB tests is restricted by the relatively less crack extension at the maximum strain energy. Fig. 10 shows that the critical strain energy release rate G is depend upon the specimen geometries, and the maximum and minimum values of G are affected by crack velocities.

In this study, the simple linear functions of the CCS-COD relations in Fig. 11 and Table 2 were applied as the static analyses of Reference 7 since more complicated functions of the CCS-COD relation did not decrease the standard error. The optimized CCS-COD relations were not sensitive to specimen geometries, loading conditions, and crack velocities.

In Table 2, the average values of the maximum CCS f_{ccso} and the critical crack opening width w_c are 1.87 MPa and 0.114 mm, respectively. The f_{ccso} and the w_c of the TPB tests are less than those of the CLWL-DCB tests, but the differences of the average f_{ccso} and the w_c are only 25 kPa and 6.6 μm, respectively. In Fig. 12, however, the lower and upper limit values of G show the clear evidence of the specimen geometry dependence of G and the crack velocity dependence of G_{max}.
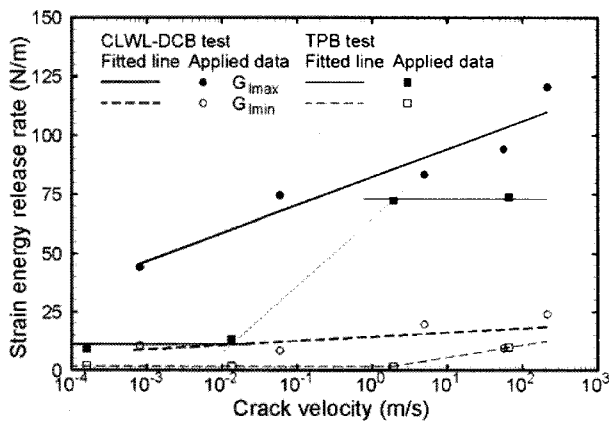
The small G_{min} of 1.78 N/m for the TPB tests except the TPB140 tests in Fig. 12 may be caused by less stress concentration around the initial notch tip than G_{min} of 14.5 N/m for the CLWL-DCB tests. The G_{min} of the fastest TPB140 tests increases to 9.81 N/m, and it may caused by faster loading-point velocity than the crack velocity.

For the CLWL-DCB tests, the crack velocity effect on G_{min} is not serious, but G_{min} increases linearly with the logarithmic value of the crack velocity $\dot{a}$ as:

$$G_{max} = 11.85 \log(\dot{a}) + 82.32 \tag{11}$$

where the units of $\dot{a}$ and G_{min} are m/s and N/m, respectively. The G_{min} of 11.2 N/m for the slow TPB tests increases suddenly to 73.0 N/m for the fast TPB tests. But the G_{min} of the TPB test is still less than that of the CLWL-DCB tests.

The fracture resistances of the CLWL-DCB tests are shown in Fig. 13. The total fracture energy rates G_f were calculated by adding $G(a)$ in Fig. 10 into $G_{fpz}(a)$. The G_{fpz} of the CLWL-DCB tests increases linearly until Step Ⓓ, and then it remains at an approximately constant value of the fracture energy density, G_{FPZ}, defined by eq. (3). Step Ⓓ of the CLWL-DCB tests is determined when the FPZ developed fully for the CCS-COD relations in Table 2, and the loading-point displacement and the crack extension of each test at Step Ⓓ are listed in Table 3. The average size of the fully developed FPZ at Step Ⓓ was 166 mm. The relatively large G_{fpz} of the DCB120 tests after Step Ⓓ was
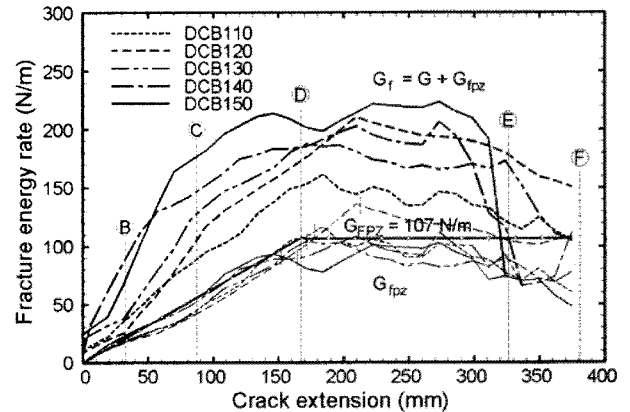

Fig. 12 Crack velocity effect on limits values of strain energy release rates.

Fig. 13 Computed resistance cruves of CLWL-DCB specimens.

Table 3 Crack extension and load-point displacement at each step (unit: mm).

Step		TPB test group					CLWL-DCB test group						Expected behavior
		110	120	130	140	Ave.	110	120	130	140	150	Ave.	
Ⓐ	a			0.0					0.0				Micro-cracking
	u_p	0.024	0.020	0.021	0.028	0.023	0.027	0.026	0.027	0.037	0.034	0.028	
Ⓑ	a			25.4			25.4	38.1	38.1	-	27.9	32.4	Micro-crack localizing
	u_p	0.056	0.054	0.068	0.066	0.061	0.044	0.054	0.062	-	0.062	0.056	
Ⓒ	a			63.5			80.7	104.4	90.1	58.4*	73.4	87.2	Maximum fracture criterion
	u_p	0.102	0.104	0.138	0.123	0.117	0.086	0.111	0.112	0.094*	0.107	0.104	
Ⓓ	a	83.6	80.3	76.2	77.0	79.3	177.8	212.9†	171.6	164.7	151.6	166.4	Full development of FPZ
	u_p	0.145	0.168	0.177	0.161	0.163	0.178	0.226†	0.194	0.196	0.185	0.188	
Ⓔ	a			-			-	330.2	330.2	292.1*	317.5	326.0	Decreasing fracture criterion
	u_p			-			-	0.379	0.372	0.319*	0.351	0.368	
Ⓕ	a			101.6					381.0				Maximum crack extension
	u_p	0.403	0.391	0.360	0.345	0.375	0.437	0.455	0.434	0.405	0.414	0.429	

*The values not included for average.

caused by the larger w_c than those of the other tests in Table 3. In Table 3, Steps Ⓐ and Ⓕ are determined from the average measured crack extensions in Fig. 5; Steps Ⓑ, Ⓒ and Ⓔ from the fracture criterion of G and Step Ⓓ at the full development of the FPZ.

For the TPB tests, the fracture resistances in Fig. 14 increases stably until Step Ⓒ, but the slope of G_{fpz} after the Step Ⓒ increases suddenly to the G_{FPZ} because of releasing the strain energy in the specimen, rather than increasing external work. From the result, the unstable crack extension after the Step Ⓒ can be expected, and the unstable increment of the load-point displacement for the static tests had been observed.[7] Thus, G_{max} of the TPB tests may be limited by the unstable crack extension. Except the TPB140 tests showing rigid motion after Step Ⓒ. The G_{fpz} of the TPB test reaches G_{max} to at about 70 mm crack extension. And then G_{fpz} increases again until the 80 mm crack extension. The larger G_{fpz} than the G_{FPZ} is only possible when the fracture energy is dissipated by crack opening in the FPZ rather then crack extension such as the decreasing crack extension rate in Fig. 5 and the increasing CTW in Fig. 10.

The size of the fully developed FPZ for the TPB tests at Step Ⓓ is only about a half of that for the CLWL-DCB tests as shown in Fig. 5 and Table 3. The relatively small size of the fully developed FPZ also explains the crack arresting behavior in the TPB specimens. The crack arresting of the TPB specimens can be expected by the highly stressed narrow compression zone in front of the crack tip occurred by the geometry of the TPB specimen.

Fig. 15 shows the singularity rate defined as G / G_f. The singularity rate increases by increasing crack velocity. The average singularity rates of the TPB test during the crack extensions are 0.24 for the slow tests and 0.54 for the TPB140 tests. The singularity rates of the CLWL-DCB tests after Step Ⓓ are constant values of 0.33 for the DCB110 tests and 0.57 for the DCB150 tests. Therefore, the singularity should be considered for the modified S-FPZ model, and the singularity rate can be used to express the quantity of the concrete brittleness for the fully developed FPZ.

5. Conclusions

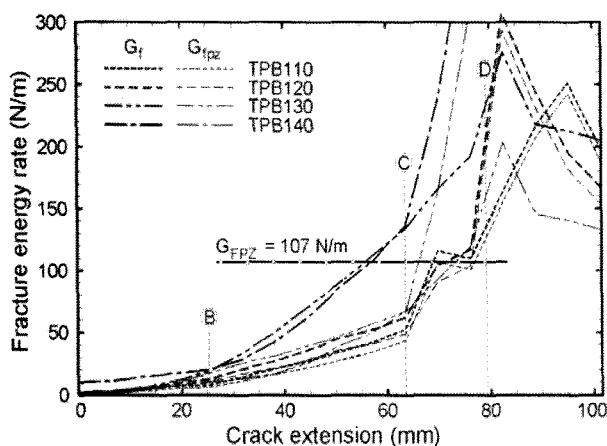The average measured responses of the TPB and CLWL-DCB

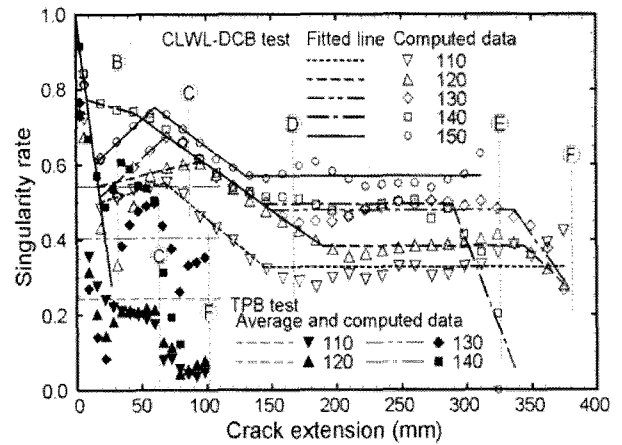**Fig. 14** Computed resistance curves of TPB specimens.

Fig. 15 Singularity rates for crack extension.

tests were analyzed by the modified S-FPZ model. The average crack velocities measured with strain gages were between 0.16~65.8 m/s for 102 mm crack extension of the TPB tests and 0.80~215 m/s for 381 mm crack extension of the CLWL-DCB tests.

The fracture properties of the modified S-FPZ model for concrete were determined by minimizing the standard error between the calculated and experimentally evaluated fracture energies.

From this study, it can be concluded that :

1) The linear CCS-COD relationships of the FPZ were independent of the specimen geometry and crack velocity. For the materials in this study, the maximum crack closure stress, the critical crack opening width and the average fracture energy density in the FPZ were 1.87 MPa, 0.114 mm and 107 N/m, respectively. In the case of CLWL-DCB tests, the fracture energy rate of the FPZ increases linearly with crack extension, until the full development of the FPZ. And then the fracture energy rate remains approximately constant value of the fracture energy density.

2) The fracture criterion of the strain energy release rate G depends on not only specimen geometry and crack velocity but also crack extension. The strain energy release rate increases from the G_{min} to the G_{max} after the 30 mm crack extension. The value of the G_{max} in the TPB tests is restricted by unstable crack extension at the maximum strain energy, whereas the G_{max} of the CLWL-DCB tests occured at the peak load. The G_{max} of the CLWL-DCB tests is proportional to logarithm of the crack velocity.

3) The initial constant value of the G_{min} may be caused by the distribution of micro-cracks, and the increasing G from the G_{min} to the G_{max} by the micro-crack localization.

4) For the CLWL-DCB specimens, the size of the FPZ was 166 mm. After the full development of the FPZ, the singularity rate G/G_f of the CLWL-DCB tests was 0.33 for the static loading and 0.57 for the crack velocity of 215 m/s.

Acknowledgements

References

1. Hillerborg, A., Modeer, M., and Petersson, P.-E., "Analysis of Crack Formation and Crack Growth in Concrete by Means of Fracture Mechanics and Finite Elements", *Cement and Concrete Research*, Vol.6, No.6, 1976, pp.773~782.

2. Bazant, Z. P. and Oh, B. H., "Crack Band Theory for Fracture of Concrete", *Materials and Structures, RILEM*, Vol.16, No.1, 1983, pp.155~177.

3. Landis, E. and Shah, S. P., "Recovery of Microcrack Parameter in Mortar Using Quantitative Acoustic Emission", *Journal of Nondestructive Evaluation*, Vol.12, No.4, 1993, pp.213~232.

4. Li, Z., "Microcrack Characterization in Concrete under Uniaxial Tension", *Magazine of Concrete Research*, Vol.48, No.176, 1996, pp.219~228.

5. Li, F. and Li, Z., "Acoustic Emission Monitoring of Fracture of Fiber Reinforced Concrete in Tension", *ACI Materials Journal, ACI*, 2000, Vol.97, No.6, pp.629~636.

6. Krstulovic-Opara, N., "Fracture Process Zone Presence and Behavior in Mortar Specimens", *ACI Materials Journal, ACI*, Vol.90, No.6, 1993, pp.618~626.

7. Yon, J. H., "Modified S-FPZ Model for a Running Crack in Concrete", *Journal of Korea Concrete Institute*, Vol. 15, No. 6, 2003, pp.802~810.

8. Yon, J. H., Hawkins, N. M., and Kobayashi, A. S., "Numerical Simulation of Mode I Dynamic Fracture of Concrete", *Journal of Engineering Mechanics, ASCE*, Vol.117, No.7, 1991, pp.1596~1610.

9. Miller, R. A., Castro-Montero, A., and Shah, S. P., "Cohesive Crack Models for Cement Mortar Examined Using Finite Element Analysis and Laser Holographic Measurement", *Journal of the American Ceramic Society*, Vol.74, No.4, 1991, pp.629~636.

10. Du, J, Yon, J. H., Hawkins, N. M., and Kobayashi, A. S., "Fracture Process Zone for Concrete for Dynamic loading", *ACI Materials Journal, ACI*, Vol.89, No.3, 1992, pp.252~258.

11. Yon, J. H., "Dynamic Fracture Behaviors of Concrete Three-Point Bend Specimens", *Journal of the Korea Concrete Institute*, Vol.14, No.5, 2002, pp.689~697.

12. Yon, J. H., "Effects of Crack Velocity on Fracture Resistance of Concrete", *Journal of the Korea Concrete Institute*, Vol.15, No.1, 2003, pp.52~59.

13. Mindess, S. and Bentur, A., "A Preliminary Study of the Fracture of Concrete Beam under Impact Loading, Using High Speed Photography", *Cement and Concrete Research*, Vol.15, No.5, 1985, pp.474~484.

14. Shah, S. P., Swartz, S. E., and Ouyang, C., *Fracture Mechanics of Concrete*, John Wiley & Sons Inc., New York, 1995, 552pp.

15. Yon, J. H., Hawkins, N. M., and Kobayashi, A. S., "Comparisons of Concrete Fracture Models", *Journal of Engineering Mechanics, ASCE*, Vol.123, No.3, 1997, pp.196~203.

16. Cook, R. D., Malkus, D. S., and Plesha, M. E. and Witt, R. J., *Concepts and Applications of Finite Elements Analysis*, 4th ed., John Wiley & Sons Inc., New York, 2002, 719pp.